Understanding the inoculation of aluminium grains during welding under the influences of high cooling rate and high temperature gradient

To cite this article: Yijiang Xu *et al* 2023 *IOP Conf. Ser.: Mater. Sci. Eng.* **1281** 012015

Understanding the inoculation of aluminium grains during welding under the influences of high cooling rate and high temperature gradient

Yijiang Xu[1], Geir Kvam-Langelandsvik[1], Ivan Bunaziv[1], Yanjun Li[2]

1. SINTEF industry, Richard Birkelands vei 3, 7034 Trondheim, Norway.

2. Department of Materials Science and Engineering, Norwegian University of Science and Technology (NTNU), N-7491 Trondheim, Norway

E-mail address: yanjun.li@ntnu.no (Yanjun Li)

Abstract. Inoculation is an important method to generate fine equiaxed grain structures in alloys during solidification, which is widely used in shape casting and direct chill casting processes of aluminium alloys. Different from the normal casting processes, welding and additive manufacturing can have ultrahigh cooling rate and temperature gradient during solidification. This makes the grain refinement by inoculation method more difficult. Therefore, a deeper understanding on the influences of cooling rate and temperature gradient on the nucleation and growth of grains is necessary. In this work, a numerical model is developed to quantitatively address the above influences. The model has been successfully applied to predict the grain size in the welding of aluminium alloys as a function of locations.

1. Introduction

Grain refinement by inoculation is widely used in shape casting and direct chill (DC) casting processes of aluminium alloys. Under such normal solidification conditions, the grain refinement behaviours including nucleation and grain growth, have been studied extensively through experimental studies and numerical modelling work in the past decades [1–11]. Among the experimental works, in-situ X-radiographic studies [10–13] have greatly contributed to the in-depth understanding of the nucleation and growth behaviours of grains in inoculated aluminium alloys. Based on the important free-growth criterion for heterogeneous nucleation of grains on potent inoculation particles proposed by Greer et al.[14], more advanced grain size prediction models for inoculated aluminium alloys have been developed in the last decade, in which the effects of addition level of grain refiners, solute concentration, cooling rate and temperature gradient have been well addressed [10,11,15,16]. The simulation results have a good agreement with the measured grain size of in-situ X-radiographic experiments.

Inoculation has also been explored in fusion welding and additive manufacturing of aluminium alloys to achieve fine equiaxed grain structure, which helps to reduce the solidification cracking and improve the mechanical properties such as strength, ductility, and toughness [17]. However, different from the normal casting, columnar grain structures are often obtained in welding and AM processes by adding normal grain refiner particles into the filler metals like wire and powder feedstock. The difficulty of grain refinement by inoculation in welding and additive manufacturing has been attributed to the much higher cooling rate and temperature gradient during solidification [18–22]. To

date, deep understanding of the effect of such solidification conditions on heterogeneous nucleation and growth of grains has been limited.

In this work, a numerical model is developed to quantitatively address the influences of high cooling rate and high temperature gradient. The model will be applied to predict the grain size of the gas metal arc welding of aluminium alloys inoculated with Ti as a function of local solidification conditions.

2. Model for grain size prediction

The numerical model used in this work is an extension to a previous grain size prediction model developed for normal directional solidification conditions [11]. A schematic drawing of the 2D cross section of solidification domain used in the model is shown in Figure 1. Constant cooling rate and temperature gradient is applied in such local domain, while the local solidification parameter could be determined by finite element simulation. The interfacial non-equilibrium solidification effect on the dendrite tip growth is taken into account by implementing growth rate dependent kinetic partition coefficient k_v and kinetic liquidus slope m_v. The temperature gradient effect on the tip radius of dendrite was also included.

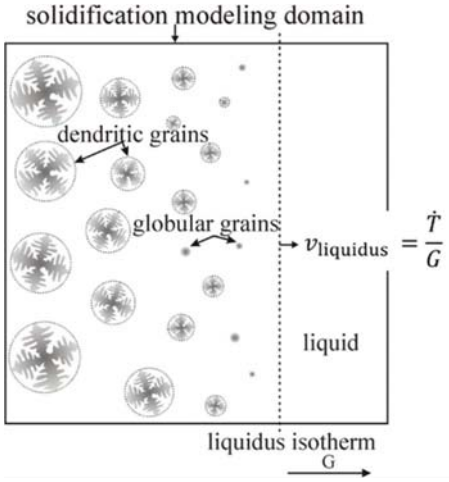

Figure 1. Schematic figure showing the 2D cross section of solidification modelling domain along the temperature gradient G direction. Nucleation and grain growth propagates from the left colder side towards the right hotter side.

The heterogeneous nucleation of grains on inoculant particles is based on the free growth criterion. The governing equations to determine the free growth undercooling and local undercooling experienced by inoculant particles, the size of inhibited nucleation zone around growing grains, and grain growth velocity were described in a previous model, and could be found in [11]. Here only some of the new equations are described.

During rapid solidification, the solute partition coefficient k_v is dependent of the moving velocity of solid/liquid interface V, and is estimated here based on [23]:

$$k_v = \frac{k + a_0 V/D_i}{1 + a_0 V/D_i} \quad (1)$$

where k is the equilibrium partition coefficient (could be assumed as constant or temperature dependent), a_0 is a characteristic length scale for solute trapping (of the order of interatomic distance), V is the growth velocity. D_i is the solute interface diffusion coefficient, which is often approximated to be the diffusion coefficient in the liquid D_l, given by the Arhenius type equation:

$$D_l = D_0 \exp\left(-Q/R_{gas}T\right) \quad (2)$$

And the velocity dependent liquidus slope m_v is calculated by the following equation [24]:

$$m_v = m\frac{1 - k_v[1 - \ln\left(\frac{k_v}{k}\right)]}{1 - k} \quad (3)$$

where m is the equilibrium liquidus slope.

For the spherical grain growth, the growth velocity is nearly the same as normal solidification condition, however, for dendritic growth, the temperature gradient will have a direct effect on the tip radius and growth rate. Here, the marginal stability criteria and Ivantsov solution [24] combining with the tip undercooling description are used to calculate the growth velocity, tip radius and tip concentration in the liquid.

Based on marginal stability criteria, the tip radius R_{tip} is [24]:

$$R_{tip} = [\frac{\Gamma}{\sigma^*(m_v G_c \xi_c - G)}]^{0.5} \quad (4)$$

Γ is the Gibbs-Thomson coefficient and σ^* is a stability constant given by $1/4\pi^2$, G is the temperature gradient. G_c is the solute concentration gradient in the liquid at the interface [25], and ξ_c is a stability parameter [24]:

$$\xi_c = 1 - \frac{2k_v}{\left[1+\left(\frac{2\pi}{Pe}\right)^2\right]^{0.5} - 1 + 2k_v} \quad (5)$$

3. Experiment

The Gas metal arc welding (GMAW) experiment was performed at SINTEF. The base metal for the investigation was an AA1070 aluminium alloy rolled plate of 3 mm in thickness. The welding wire was prepared by metal screw extrusion where elemental Ti powders were added into commercial purity Al (CP Al, 99.7 wt.%). The Ti composition in the welding filler wire was estimated around 0.85 wt.%. Welding was performed with I-groove geometry, with welding speed of 10 mm·s^{-1}. Due to the dilution by base metal during welding, the final titanium content in the weld decreases relative to the original wire content. The chemical compositions of the weld zone were determined by Electron Probe Micro Analyser (EPMA) and listed in Table 1.

Table 1: Chemical compositions of different experimental materials, all in wt.%.

State	Al	Fe	Si	Ti	Ni	B
CP Al	99.83	0.12	0.04	0.00	0.003	0.00
Extruded Wire	98.98	0.12	0.04	0.85	0.003	0.00
Base metal AA1070	99.70	0.20	0.08	0.01	0.002	0.00
Weld	99.54	0.12	0.01	0.32	0.002	0.00

After welding, the weld part was cut transversally to the welding direction at the mid-length to obtain vertical cross section of metallographic samples. The sample was ground, polished mechanically, and etched anodically with a solution containing 5% HBF_4 and 95% H_2O to reveal the grain structure. Micrographs were made with an optical microscope using polarized light. The grain size at three locations was measured based on the circular intercept method described in ASTM E112-13.

4. Results and discussion

The grain structure in the cross section of welds can be seen in Figure 2. For the reference sample without adding Ti in the wire, the grain structure shown in Figure 2a shows a mixture of large columnar grains grow from the weld boundary and equiaxed grain in the weld centre. In comparison, the weld with adding Ti show mainly fine equiaxed grain structure, confirming that the Ti addition in the welding filler wire has a significant grain refinement effect. For grain size measurement, three locations were selected, i.e., at weld centerline, a mid-way section, and the transition area close to the

weld boundary towards the base plate. These local areas are marked as '1', '2', and '3' in Figure 2, and the corresponding high magnification images are shown in Figure 3. As can be seen, the grains in area 1 show slightly elongated grain morphology, while they are equiaxed in the area 2 and area 3. The measured grain size from each area can be found in Table 2. It can seen that the grain size decreases from the weld boundary in area 1 to the weld centre in area 3.

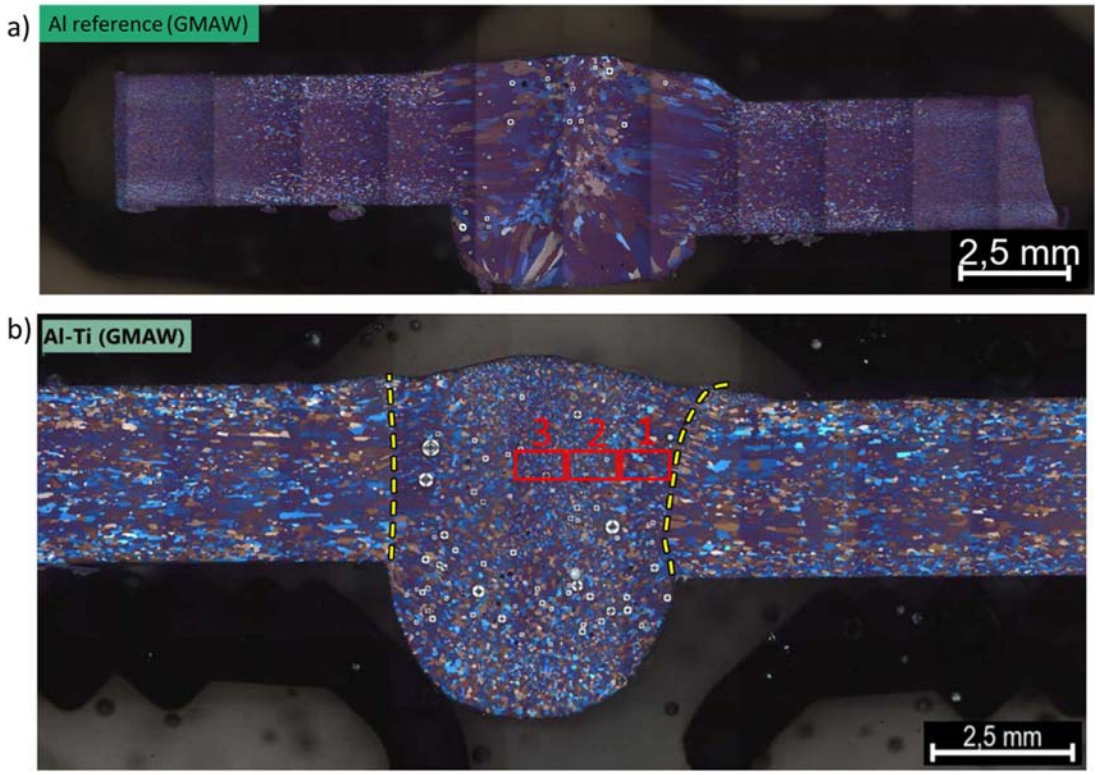

Figure 2. Optical microscope image of the cross section of the weld metal after anodization (a) The reference without adding Ti in the wire and (b) the one adding Ti in the wire. The three areas marked as 1, 2 and 3 in (b) were used for grain size measurement. The yellow dash lines indicate the melt pool boundary.

To obtain the local cooling rate and temperature gradient of the gas metal arc welding, temperature field simulation by the finite element modelling using the Abaqus software (2021 version) was performed. Such model has been validated with welding of steels [26,27]. The weld pool shape was modelled based on the experimental results of inoculated weld, as shown in Figure 2b with corresponding dimensions. The heat transfer modelling was done using DFLUX subroutine programmed in Fortran. The volumetric 3D heat source was the Goldak double ellipsoidal. The mesh was hex-dominated elements (DC3D8 type an 8-node linear heat transfer brick) of number 284 400. Temperature-dependent thermo-physical properties were applied: thermal conductivity for solid material was 210 $W \cdot m^{-1} \cdot K^{-1}$ and 100 for liquid $W \cdot m^{-1} \cdot K^{-1}$, density 2700 $kg \cdot m^{-3}$ (for liquid 2200 $kg \cdot m^{-3}$), latent heat of fusion 396 000 $J \cdot kg^{-1} \cdot K^{-1}$, and specific heat capacity for solid/liquid was 921/1050 $J \cdot kg^{-1} \cdot K^{-1}$ respectively. The temperature evolution under transient welding mode is shown in Figure 4.

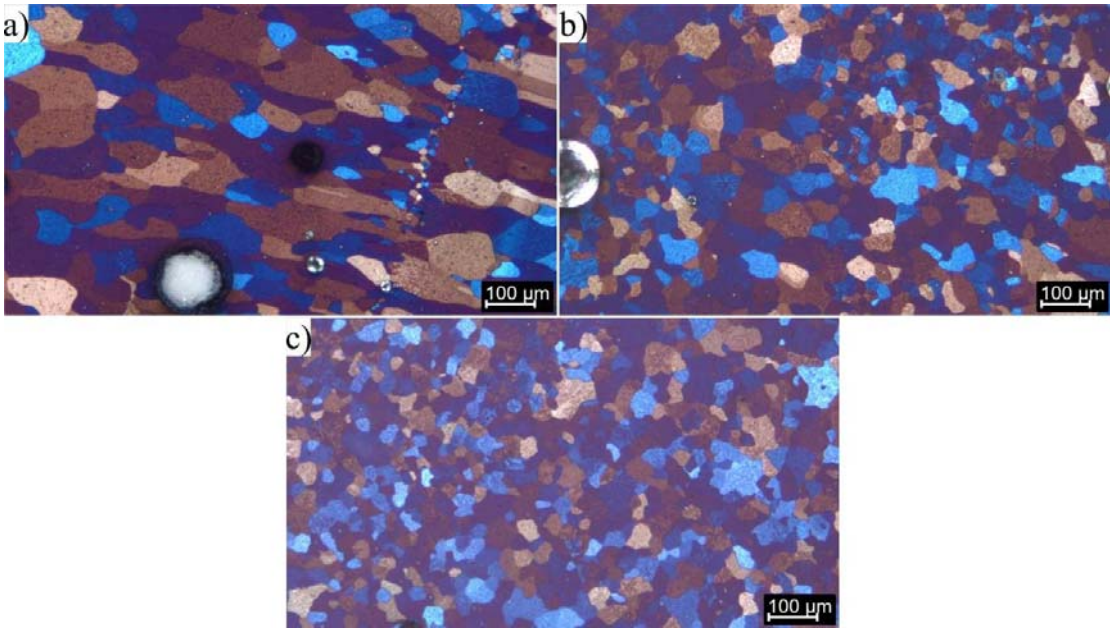

Figure 3. Optical microscope image of inoculated Al weld at three areas marked in Figure 2: (a) area 1, (b) area 2, and (c) area 3.

Table 2: Average grain size measured at three areas (marked as 1,2 and 3 in Figure 2) of inoculated aluminium weld.

Area	Average grain size [µm]	Standard deviation [µm]
1(weld boundary)	53.5	14.9
2 (midpoint of 1 and 3)	28.1	4.9
3 (weld centreline)	23.9	3.2

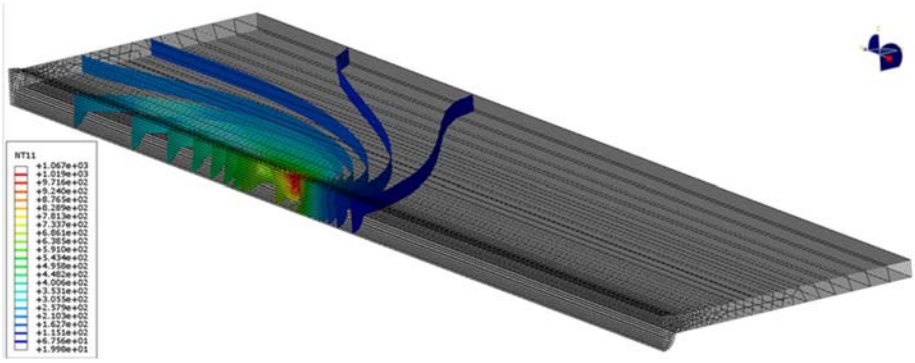

Figure 4. Temperature modelling and mesh outlook of the model during transient fusion welding.

The thermal cycle was extracted from the six locations of the weld pool at the cross section, as indicated in Figure 5a, with corresponding thermal cycle curves shown in Figure 5b. As can be seen, Point 1 close to the melt pool boundary has the lowest peak temperature, 679.4 ºC, slightly higher than

the melting point of the weld metal (~660 °C); while point 3 in the center reaches the highest peak temperature. Besides, there are plateaus in the cooling stage for some locations, such as point 2, 5 and 3, indicating the effect of latent heat release. Based on these thermal curves, the cooling rate close to the liquidus temperature and the local temperature gradient could be measured. The results are shown in Table 3. It shows that there is a big difference in cooling rate and temperature gradient at different locations in the weld and both decreases from the melt pool edge to the center of weld. These extracted data was used as input for the grain size prediction model.

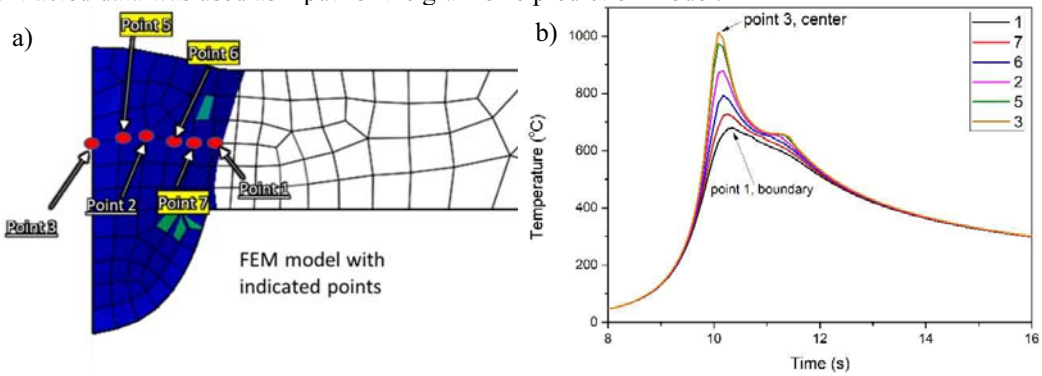

Figure 5. (a) Six node positions of weld pool cross section in Abaqus FEM model (from point 1 at the melt pool boundary to the center point 3) and (b) their corresponding thermal cycle curves as a function of time.

Table 3. Cooling rate close to the liquidus temperature and the local temperature gradient determined from the thermal cycle curves by Abaqus finite element simulation

Location	Cooling rate (K/s)	Temperature gradient (K/mm)
1	103	51.6
2	84	11.4
3	58	2.0

To simplify the influences of different solute contents in the weld on the growth kinetics of grains during solidification, the weld metal is simplified as a binary Al-0.322Ti (wt.%) alloy based on equivalent total growth restriction factor, $Q = \sum m_i Ci * (k_i - 1)$, where Ci is the concentration of solute element I, since Ti has the highest contribution to the Q value and the lowest diffusivity in liquid Al. The nucleant particles are in-situ formed Al_3Ti [28] before peritectic reaction. At the nucleation stage of Al grains, the total Ti solute is considered as the maximum solubility of Ti in liquid Al, 0.15 wt.%, which is used in the model for grain growth. The total volume fraction of the Al_3Ti particles is calculated as 0.362% based on the real Ti content in the weld. It is assumed that they have a log-normal particle size distribution [10], same as TiB_2 particles in Al-Ti-B refiner:

$$\frac{N(d)}{N_0} = \frac{\Delta d}{\sigma d\sqrt{2\pi}} exp\left(-\frac{(ln(d) - ln\,(d_0))^2}{2\sigma^2}\right) \quad (6)$$

where $N(d)$ is the number of particles with diameter between d and $d + \Delta d$, N_0 is the total number of TiB_2 particles, the ratio $\frac{N(d)}{N_0}$ is the relative population, d_0 =0.77 μm is the geometric mean of distribution and σ=0.5 is the geometric standard deviation. It is shown in Figure 6a. Besides, the total

volume fraction, the size distribution and the total number density are considered independent of cooling rate studied here.

Figure 6b shows the grains size predicted by the current model in comparison to the experimental measurement shown in Table 2 at three locations of Al-Ti weld. The total number density of the Al_3Ti particles formed during solidification is an unknown parameter and thus has to be tuned based on grain size data at one of the locations, here location 1. Then this value is fixed and used as input for grain size simulation in location 2 and location 3. As can be seen, the grain size predicted by the model has a good agreement with the experimental results. From location 1 to location 3, the grain size decreases although the cooling rate (shown in Table 3) decreases as well. It reveals that the local temperature gradient has a greater influence than local cooling rate on the nucleation of Al grains in the weld pool. The larger grain size in location 1 is due to the larger temperature gradient, while smaller grain size in location 3 is promoted by smaller temperature gradient. Such agreement verifies that the model is able to simulate the effects of cooling rate and temperature gradient in welding of Al alloys on the grain size evolution and distribution.

Besides, the Al welding without adding Ti could also be simulated by the present model, assuming a small value of total number density of particles, for example typical amount of 0.1 wt.% addition of Al-Ti-B. The simulation results under solidification condition of location 1 show that the nucleation of new grains are not possible any more after first class nucleation at the melt boundary, indicating that columnar grains will form and grow towards the weld centre, which is in a good agreement with the experimental results presented in Figure 2.

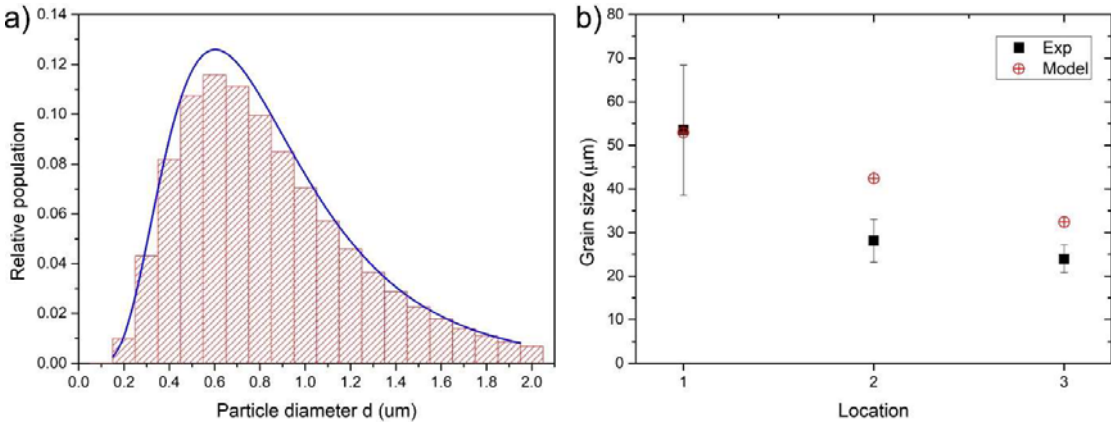

Figure 6. (a)Log-normal size distribution of Al_3Ti particles used for the simulation. (b) Grain size predicted by the current model, in comparison to the experimental results. The location should be referred to the ones marked in Fig. 2, where 1 is at the edge while 3 is at the centre of weld.

The possible change of non-equilibrium solute partition coefficient k_v and non-equilibrium liquidus slope m_v under current welding conditions have been investigated. Typical growth velocity evolution during solidification, for example, of the first class of grains nucleated in the melt at location 1, location 2 and location 3 is plotted in Figure 7a. As can be seen, the growth velocity will start from a very small value, then increase as solidification time increases (undercooling increase as well), and finally may reach a maximum value and then decreases again due to solute segregation effect of the residue melt. The corresponding non-equilibrium solute partition coefficient k_v, and non-equilibrium liquidus slope m_v at the growth interface are shown in Figure 7b and Figure 7c. It can be seen that k_v decrease slightly from 7 to about 6.98 at solidification condition of location 1, while in another two cases, it may decrease to 6.92. Nevertheless, the change of k_v is those conditions are not big. For mv shown in Figure 6c, the change is even less obvious. It could be concluded that k_v and m_v are not influenced much by the cooling rate and temperature gradient in common welding condition.

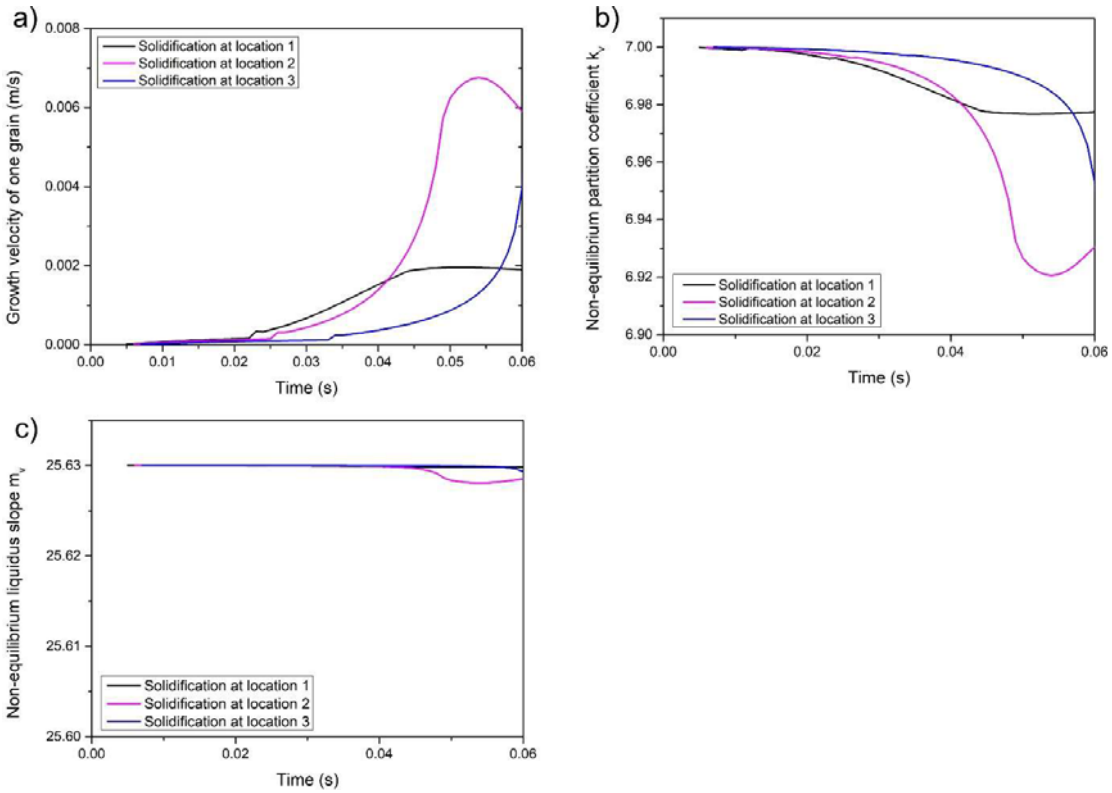

Figure 7. (a) Grain growth velocity of the first class of grains nucleated in the melt solidified at location 1, location 2 and location 3; (b) corresponding non-equilibrium solute partition coefficient k_v, (c) corresponding non-equilibrium liquidus slope m_v.

5. Conclusions

A numerical model was developed to quantitatively address the effect of high cooling rate and high temperature gradient on the heterogeneous nucleation and grain size of Al alloys during solidification. The model has been applied to the gas metal arc welding of aluminium alloys inoculated with Ti. By the finite element simulation of the temperature field, local cooling rate and temperature at different locations at the weld metal was obtained. The model has successfully predicted the grain size variation at those locations as a function of cooling rate and temperature gradient. It shows a good agreement with the measurement data of the welding experiment. It is found that, under the solidification condition of welding, the local temperature gradient in the welding pool has a more important influence on the heterogeneous nucleation of grains and therefore the final grain size. However, it can be expected that solidification conditions of additive manufacturing will have much more influences. It if worth of testing the validity of the model for the AM processes of aluminium alloys in a future work.

Acknowledgement

This research work has been funded by the SFI PhysMet, (Centre for Research-based Innovation, 309584). The authors gratefully acknowledge the financial support from the Research Council of Norway and the partners of the SFI PhysMet.

References

[1] Murty B S, Kori S A and Chakraborty M 2002 Grain refinement of aluminium and its alloys by heterogeneous nucleation and alloying *Int. Mater. Rev.* **47** 3–29
[2] Quested T E 2004 Understanding mechanisms of grain refinement of aluminium alloys by inoculation *Mater. Sci. Technol.* **20** 1357–69
[3] Easton M A, Qian M, Prasad A and StJohn D H 2AD Recent advances in grain refinement of light metals and alloys *Curr. Opin. Solid State Mater. Sci.* **20** 13–24
[4] Greer A L 2016 Overview: Application of heterogeneous nucleation in grain-refining of metals *J. Chem. Phys.* **145** 14
[5] Fan Z, Wang Y, Zhang Y, Qin T, Zhou X R, Thompson G E, Pennycook T and Hashimoto T 2AD Grain refining mechanism in the Al/Al–Ti–B system *Acta Mater.* **84** 292–304
[6] Iqbal N, van Dijk N H, Offerman S E, Moret M P, Katgerman L and Kearley G J 6AD Real-time observation of grain nucleation and growth during solidification of aluminium alloys *Acta Mater.* **53** 2875–80
[7] StJohn D H, Qian M, Easton M A and Cao P 7AD The Interdependence Theory: The relationship between grain formation and nucleant selection *Acta Mater.* **59** 4907–21
[8] Shu D, Sun B, Mi J and Grant P S 3AD A quantitative study of solute diffusion field effects on heterogeneous nucleation and the grain size of alloys *Acta Mater.* **59** 2135–44
[9] Du Q and Li Y J 2014 An extension of the Kampmann-Wagner numerical model towards as-cast grain size prediction of multicomponent aluminum alloys *Acta Mater.* **71** 380–9
[10] Xu Y, Casari D, Du Q, Mathiesen R H, Arnberg L and Li Y 2017 Heterogeneous nucleation and grain growth of inoculated aluminium alloys: An integrated study by in-situ X-radiography and numerical modelling *Acta Mater.* **140** 224–39
[11] Xu Y, Casari D, Mathiesen R H and Li Y 2018 Revealing the heterogeneous nucleation behavior of equiaxed grains of inoculated Al alloys during directional solidification *Acta Mater.* **149** 312–25
[12] Murphy A G, Mathiesen R H, Houltz Y, Li J, Lockowandt C, Henriksson K, Melville N and Browne D J 11AD Direct observation of spatially isothermal equiaxed solidification of an Al–Cu alloy in microgravity on board the MASER 13 sounding rocket *J. Cryst. Growth* **454** 96–104
[13] Murphy A G, Mirihanage W U, Browne D J and Mathiesen R H 8AD Equiaxed dendritic solidification and grain refiner potency characterised through in situ X-radiography *Acta Mater* **95** 83–9
[14] Greer A L, Bunn A M, Tronche A, Evans P V and Bristow D J 6AD Modelling of inoculation of metallic melts: application to grain refinement of aluminium by Al–Ti–B *Acta Mater.* **48** 2823–35
[15] Xu Y, Casari D, Mathiesen R H and Li Y 2019 Revealing the Heterogeneous Nucleation and Growth Behaviour of Grains in Inoculated Aluminium Alloys During Solidification TMS 2019 148th Annual Meeting & Exhibition Supplemental Proceedings (Cham: Springer International Publishing) pp 1665–75
[16] Xu Y, Du Q and Li Y 2015 Influence of Dendritic Growth of Equiaxed Grains on As-Cast Grain Size Prediction of Inoculated Aluminum Alloys *Trans. Indian Inst. Met.* **68** 1013–6
[17] Schempp P, Cross C E, Pittner A and Rethmeier M 2013 Influence of Solute Content and Solidification Parameters on Grain Refinement of Aluminum Weld Metal *Metall. Mater. Trans. A* **44** 3198–210
[18] Schempp P 2013 Grain refinement in aluminium GTA welds
[19] Li X P, Ji G, Chen Z, Addad A, Wu Y, Wang H W, Vleugels J, Van Humbeeck J and Kruth J P 2017 Selective laser melting of nano-TiB2 decorated AlSi10Mg alloy with high fracture strength and ductility *Acta Mater.* **129** 183–93

[20] Xiao Y K, Bian Z Y, Wu Y, Ji G, Li Y Q, Li M J, Lian Q, Chen Z, Addad A and Wang H W 2019 Effect of nano-TiB2 particles on the anisotropy in an AlSi10Mg alloy processed by selective laser melting *J. Alloys Compd.* **798** 644–55
[21] Tan Q, Zhang J, Sun Q, Fan Z, Li G, Yin Y, Liu Y and Zhang M-X 2020 Inoculation treatment of an additively manufactured 2024 aluminium alloy with titanium nanoparticles *Acta Mater.* **196** 1–16
[22] Tan Q, Zhang J, Mo N, Fan Z, Yin Y, Bermingham M, Liu Y, Huang H and Zhang M-X 2020 A novel method to 3D-print fine-grained AlSi10Mg alloy with isotropic properties via inoculation with LaB6 nanoparticles *Addit. Manuf.* **32** 101034
[23] Aziz M J 1982 Model for solute redistribution during rapid solidification *J Appl Phys* **53** 1158–68
[24] Kurz W, Giovanola B and Trivedi R 1986 Theory of microstructural development during rapid solidification *Acta Metall.* **34** 823–30
[25] Frenk A and Kurz W %J L in E 1992 Microstructure formation in laser materials processing **1** 193–212
[26] Bunaziv I, Akselsen O M, Frostevarg J and Kaplan A F H 2018 Laser-arc hybrid welding of thick HSLA steel *J. Mater. Process. Technol.* **259** 75–87
[27] Bunaziv I, Wenner S, Ren X, Frostevarg J, Kaplan A F H and Akselsen O M 2020 Filler metal distribution and processing stability in laser-arc hybrid welding of thick HSLA steel *J. Manuf. Process.* **54** 228–39
[28] Maxwell I and Hellawell A 2AD A simple model for grain refinement during solidification *Acta Met.* **23** 229–37